Unified picture of structural relaxation, beta relaxation, and excess wing in glass formers

Chun-Shing Lee,[1] Hai-Yao Deng,[2] Linghan Zhang,[3] Chu Xiao,[1] Bo Li,[1,*] Cho-Tung Yip,[1,†] and Chi-Hang Lam[3,‡]
[1]*Department of Physics, Shenzhen Graduate School, Harbin Institute of Technology, Shenzhen 518055, China*
[2]*School of Physics and Astronomy, Cardiff University, 5 The Parade, Cardiff, Wales CF24 3AA, United Kingdom*
[3]*Department of Applied Physics, Hong Kong Polytechnic University, Hong Kong, China*

(Received 7 May 2025; revised 25 June 2025; accepted 1 October 2025; published 23 October 2025)

We study the microscopic origins of relaxation modes revealed by spectroscopic studies of glasses. Major features in calorimetric and structural relaxation spectra, including α peaks, β peaks, and excess wings, are reproduced using a distinguishable-particle lattice model. It is based on void-induced particle hops, which model stringlike particle hopping motions. Excess wings are found to be flattened variants of β peaks when particle hopping barriers admit a wide distribution. A β relaxation event is attributed to the hop of a particle which neighbors a void. An α relaxation event involves a similar process by an arbitrary particle but also includes, as a prior step, the arrival of a diffusing void to become its neighbor.

DOI: 10.1103/kx3x-c8n1

Spectroscopy is a cornerstone of physics, providing insights into the dynamics of physical systems. For structural glasses [1–6], spectroscopy typically shows a main peak named the α relaxation peak. Many glasses also exhibit a higher-frequency Johari-Goldstein (JG) β peak [7,8], originally identified in dielectric spectroscopy but are also observed using other methods such as dynamic mechanical spectroscopy (DMS) [9]. Despite the relatively universal properties of the α peaks across various glass formers, the β peaks can be more pronounced or broadened and can even be replaced by excess wings [9–14]. Such diversity was found to be related to the behavior of the enthalpy of mixing in metallic glasses [5,15]. To explain α relaxation and related physics, thermodynamic theories are widely investigated [2,3] while dynamical facilitation [1,2] has also been gaining much recent attention [16–18]. In contrast, although β relaxation is often regarded as a precursor to α relaxation [4], its possible explanations seldom qualify as intrinsic or essential parts in the major theories [1–3]. Microscopically, stringlike motions dominating particle dynamics in molecular dynamics (MD) simulations are most often attributed as α relaxation [19,20], but have also been suggested as β relaxation [21,22]. Understanding the microscopic mechanisms behind the major spectral features is essential to understand glass.

In this article, we will study dynamical spectra of glass using a distinguishable-particle lattice model (DPLM) [23] and we demonstrate that α peaks, β peaks, and excess wings can all be reproduced. The microscopic mechanisms of the associated relaxations and their relations are elucidated.

I. METHODS

A. The model

The DPLM simulates particle hopping motions induced by voids, the relevance of which was supported by previous studies [24–27]. Each hop represents a microstring, i.e., a coherent stringlike particle hopping motion [19,28], albeit a trivial string length of one particle. Multiple hops of a void extend a microstring into a longer incoherent string [22], closely resembling those from MD simulations [21,29,30]. The model can reproduce many thermodynamic [31–34] and kinetic [23,35–39] features of glass. In particular, it can simulate both strong and fragile glasses [35]. Here, we follow the definitions in [35] with generalizations in some simulations to be explained later.

We define our DPLM in two dimensions (2D) on a square lattice of linear dimension $L = 100$. Each particle has its own unique type and there is a small fraction ϕ_v of unoccupied sites modeling voids. Periodic boundary conditions are imposed. Nearest-neighboring particles k and l interact with a particle-dependent pair-interaction energy V_{kl} which is quenched in a simulation. It is sampled from the distribution [35]

$$g(V) = G_0 + (1 - G_0)\delta(V - 0.5),\ V \in [-0.5, 0.5], \quad (1)$$

where G_0 controls the fragility and δ denotes the Dirac delta function. The physical relevance of G_0 is explained in detail in Ref. [35]. Specifically, it governs the temperature dependence of the system entropy, reflecting how the number of energetically favorable hopping pathways varies with temperature. A small G_0 leads to a sharp decrease in entropy even with a slight reduction in temperature, strongly suppressing the dynamics and resulting in a fragile system.

As such, a particle is usually bonded with four nearest-neighboring particles, fewer if it is neighbored by a void. This aligns with the lower averaged bond order observed closeby to strings in realistic system [29,30].

The total energy of the system is defined by $E = \sum_{\langle i,j\rangle'} V_{s_i s_j}$, where s_i is the particle located at site i and the sum is restricted to nearest-neighboring occupied sites i and j. The kinetics is defined by allowing particle l to hop to a nearest-neighboring void, if any, with a rate w_l given by

$$\mathrm{w}_l(\Delta E) = \mathrm{w}_0 \exp\left[-\frac{E_0 + U_l + \max(\Delta E, 0)}{k_B T}\right], \quad (2)$$

*Contact author: libo2021@hit.edu.cn
†Contact author: h0260416@hit.edu.cn
‡Contact author: c.h.lam@polyu.edu.hk

where $w_0 = 10^6$, $k_B = 1$ is the Boltzmann constant, ΔE equals the system energy change due to the hop, $E_0 + U_l$ is an energy barrier offset, and T is the bath temperature. Hence, detailed balance is satisfied and the system energy approaches its equilibrium value upon kinetic Monte Carlo simulation at a constant temperature.

B. Calorimetric spectroscopy

Different spectroscopic methods often give closely analogous results on glass [40]. We study calorimetric spectroscopy [41,42] which, like other thermal analysis [31,33,34,36], is easily applicable to the DPLM. To study calorimetric spectroscopy, we perform a step cooling perturbation to initially equilibrium systems, following methods commonly used in spectroscopic approaches [4,40]. For a nominal temperature T, a DPLM system is first equilibrated at temperature $T_i = (1 + \delta_T/2)T$ by direct construction [23]. Then, we perturb the bath temperature at time $t = 0$ abruptly to $T_f = (1 - \delta_T/2)T$ with a percentage temperature change $\delta_T = 6\%$. We then continuously measure the system energy $E(t)$ at time t in further simulations. We calculate the average particle energy $e(t) = E(t)/N$, where N denotes the number of particles in the system. The energy relaxation function ϕ_e is then defined as

$$\phi_e(t) = \frac{e(t) - e_f}{e_i - e_f}, \tag{3}$$

where e_i (e_f) is the average particle energy at equilibrium at T_i (T_f), which we calculate exactly [23].

Based on Eq. (3) and following similar definitions given in Ref. [4], we compute the calorimetric relaxation spectrum, i.e., the calorimetric loss, C_v'' as

$$C_v''(\omega) = \mathrm{Im}\left[\int_0^\infty dt\; e^{-i\omega t}\dot{\phi}_e(t)\right], \tag{4}$$

where ω denotes the frequency, $\dot{\phi}_e$ denotes the time derivative of ϕ_e, and "Im" takes the imaginary part.

We employ the single down-jump temperature protocol analogous to Kovacs' seminal experiment [43], except for a small jump magnitude. This protocol triggers particle reconfiguration governed by void-induced hopping dynamics [36], wherein particles continually update their pair interactions whenever they get new neighbors. This process persists as the system reaches equilibrium, characterized by a particle configuration where realized values of pair interaction V follow the equilibrium distribution $p_{eq}(V)$ (see Appendix A for details).

II. RESULTS

A. Spectral peaks and wings

We now report our results for calorimetric spectroscopy and will first consider a simple particle independent offset $E_0 = 1.5$ with $U_l \equiv 0$ following Ref. [35]. We measure the imaginary part C_v'' of the heat capacity at frequency ω according to Eq. (4). Figure 1(a) shows the calorimetric relaxation spectra computed against a wide range of frequency ω, as enabled by superior computational efficiency of lattice models. A void density $\phi_v = 1\%$ is considered. We observe clear α peaks at all T. They are asymmetric and follow the power laws $C_v'' \sim \omega$ and $C_v'' \sim \omega^{-0.6}$ on the low- and high-frequency sides, respectively, consistent with findings in experiments [14,44,45] and MD simulations [16]. The exponent -0.6 on

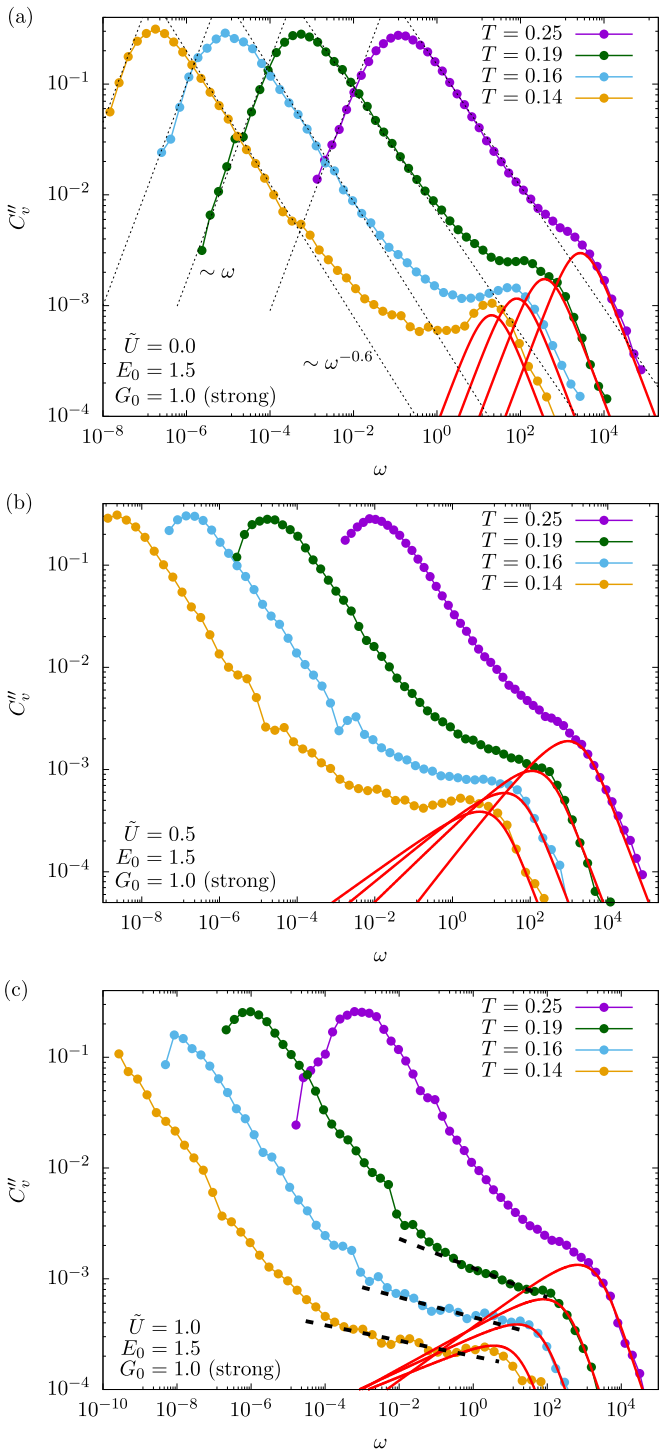

FIG. 1. Calorimetric relaxation spectra C_v'' at various temperatures T for moderately strong glass ($G_0 = 1$) with a void density $\phi_v = 0.01$ and a barrier-offset fluctuation $\tilde{U} = 0$ (a), 0.5 (b), and 1 (c). We observe α peaks in (a)–(c), β peaks in (a) and (b), and excess wings (black dashed lines) in (c). (a)–(c) Analytic prediction C_{TLS}'' (red lines) from Eq. (7) shows agreement with C_v'' at high ω. (a) $C_v'' \sim \omega$ and $C_v'' \sim \omega^{-0.6}$ (black dotted lines) are aids to the eyes.

the high-frequency side is also related to the stretching relaxation exponent reported in the energy relaxation function in Fig. 7 in Appendix A. Aside from stretched exponential relaxations, glassy systems can also exhibit compressed relaxation dynamics typically under nonequilibrium conditions [46–48] which is interesting but have not yet been reproduced by the DPLM and further nonequilibrium studies are required.

We also observe β peaks or excess wings depending on the hopping barriers. From Fig. 1(a), a high-ω shoulder emerges and sharpens into a distinct peak as T decreases. This secondary peak, or its broadened form to be discussed below, is present at sufficiently low temperatures in all our simulations and we identify it as the JGβ relaxation [49]. Note that their widths are narrower than typical ones in experiments [10,11] and simulations [21,50], a feature due to a narrow distribution of particle hopping barriers $E_0 + \max(\Delta E, 0)$ assumed in Eq. (2) with $U_l \equiv 0$. In fact, particle hopping barriers have been found to admit large fluctuations [51] and can depend on the bond types [38]. We now enlarge the barrier fluctuations in the DPLM accordingly. As randomness in the barriers must be quenched for any given particle configuration for modeling glasses, a simple effective approach is to introduce a particle dependent barrier offset U_l for particle l in Eq. (2) following, e.g., an exponential distribution [51]

$$f(U_l) = \frac{1}{\tilde{U}} e^{-U_l/\tilde{U}}, \quad U_l \geqslant 0 \tag{5}$$

with a parameter $\tilde{U}$ representing both the mean and standard deviation of this distribution. Figure 1(b) shows the spectra at $\tilde{U} = 0.5$, revealing broadened β peaks. Results qualitatively resemble dielectric spectra of, e.g., a butoxy-propanol [11]. At an even larger $\tilde{U} = 1$, the peaks as shown in Fig. 1(c) are further broadened into features resembling excess wings [12]. This trend is consistent with experimental observations in metallic glasses in which a narrower distribution of mixing enthalpy among various pairs of constituent atoms leads to more pronounced β peaks [5,15]. In contrast, varying $\tilde{U}$ does not affect the geometric characteristics of the α peaks as shown in Figs. 1(a)–1(c). In addition, we believe that $\delta_T = 6\%$ used here corresponds to the linear perturbation regime (see Appendix B).

B. Relaxation mechanisms

We now suggest the microscopic origins of the spectral peaks based on real-space particle and void dynamics. For duration t, we study the particle displacement profile $d(\vec{x}, t)$ at position $\vec{x}$ starting from its initial position $\vec{x}_0$ at time $t = 0$ when the temperature perturbation occurs, which is defined as

$$d(\vec{x}, t) = |\vec{x} - \vec{x}_0|. \tag{6}$$

Consider $T = 0.14$ and $\tilde{U} = 0$ for which a clear β peak is observed. Figure 2 shows the profiles at relaxation times $\tau_\beta = 1/\omega_\beta \simeq 0.05$ and $\tau_\alpha = 1/\omega_\alpha \simeq 5.5 \times 10^6$, where ω_β and ω_α are the peak positions obtained from Fig. 1(a) by fits to the Debye formula [52].

At τ_β, we see from Fig. 2(a) that only some particles immediately adjacent to the voids have hopped while nearly all others are stationary. This supports the picture that single hops of voids are responsible for the β relaxation. To further justify this, we analyze a simplified model of two-level systems (TLS) in which only particles initially ($t = 0$) neighboring the voids can perform single hops. At the very low T studied, most hops correspond to short-lived excitations and are reversed momentarily so that the DPLM reduces to a set of noninteracting TLSs [33]. The relaxation spectrum is then given exactly by (see Appendix C 2 for derivation)

$$C''_{\rm TLS}(\omega) = \frac{\phi_v z}{(1-\phi_v)} \left\langle \frac{\mathrm{w}_l(\Delta E)\omega}{\omega^2 + R_l{}^2(\Delta E)} \right\rangle, \tag{7}$$

where $z = 4$ is the coordination number, $R_l(\Delta E) = \mathrm{w}_l(\Delta E) + \mathrm{w}_l(-\Delta E)$ is the relaxation rate of a TLS, and the average is over the z possible single hops of all voids. Figure 1 has plotted $C''_{\rm TLS}(\omega)$ evaluated numerically using Eq. (7) without any tunable parameter. We observe a good

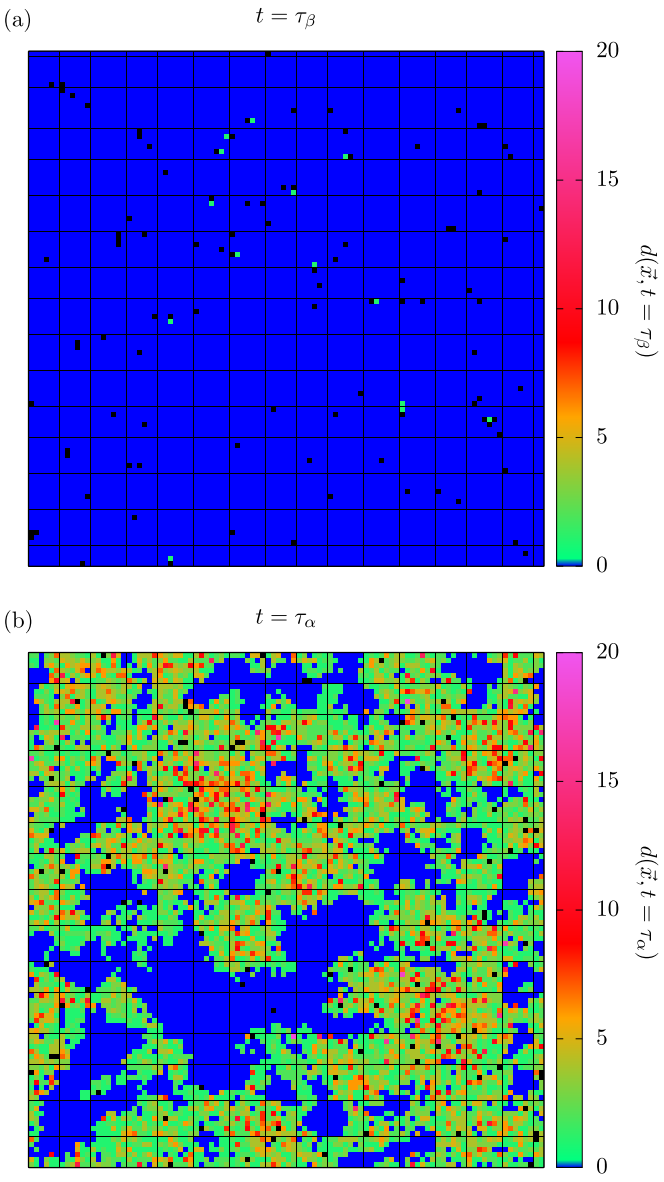

FIG. 2. Particle displacement profiles $d(\vec{x}, t)$ over duration $t = \tau_\beta$ (a) and τ_α (b) for $T = 0.14$ under the same conditions as in Fig. 1(a). Stationary particles are shaded in blue and black squares show the final void positions.

agreement, i.e., $C_v''(\omega) \simeq C_{\rm TLS}''(\omega)$, at the high-frequency side of the β peak with the peak position ω_β well predicted. For $\omega \lesssim \omega_{\rm JG}$ on the low-frequency side of the β peak, $\varepsilon''(\omega)$ reduces from the peak value because many TLSs are already relaxed at time $t \simeq \tau_\beta$ by single hops of voids. At long time, back-and-forth hopping motions within the TLSs continue which, however, lead to no further relaxation and hence little contribution to the spectral value at low frequency. The β peak being a distinct peak, as opposed to only a shoulder, is thus correlated with back-and-forth motions also known to be important at low T [22,53]. As the frequency decreases further from the β peak, the TLS approximation breaks down with $C_v''(\omega) \gg C_{\rm TLS}''(\omega)$ due to relaxation by double and further hops of voids. According to Eq. (7), the β peak is located at ω_β which approximately equals the most probable hopping rate among the successful hops of the voids (see Appendix C 3).

At τ_α, Fig. 2(b) shows that many particles, including those not initially neighboring any void, have hopped. The peak position ω_α is thus dictated by the hopping rate of all hopped particles as expected. Note, however, that $\omega_\alpha \ll \omega_\beta$ because particles not neighboring any void initially are much slower to hop and this will be further explained in Sec. III.

C. Temperature-dependent void density and equilibrium studies

As an alternative to calorimetric spectral measurements involving temperature perturbations, we have also studied structural relaxation spectra based on the self-intermediate scattering function (SISF) at equilibrium. The SISF is calculated as

$$F_s(t) = \left\langle e^{i\vec{k}\cdot(\vec{x}_l(t)-\vec{x}_l(0))} \right\rangle, \tag{8}$$

where $\vec{x}_l(t)$ denotes the position of particle l at time t, $k = 2\pi/\lambda$ with $\lambda = 2$, and the average is taken over particles, definitions of initial time $t = 0$, and independent runs. Figure 3 shows the time evolution of $-\ln F_s$ for both $G_0 = 1$ (moderately strong glass) and $G_0 = 0.01$ (fragile glass) for a T-dependent void density

$$\phi_v = \phi_v^\infty e^{-E_v/k_B T} \tag{9}$$

and $E_0 = 3$. Here, the parameters are set to $\phi_v^\infty = 0.635$ and $E_v = 0.675$ (the free energy cost of a void) so that ϕ_v ranges from 0.5% at $T = 0.14$ to 54% at $T = 4$. As T decreases, a plateau associated with β relaxation emerges and results at a two-step relaxation. For fragile glass, an additional secondary plateau emerges at very low temperature, which corresponds to a slow β, i.e., β_s, relaxation, to be discussed below. Using F_s, the structural relaxation spectrum χ'' is computed as

$$\chi''(\omega) = {\rm Im}\left[\int_0^\infty dt\, e^{-i\omega t} \dot{F}_s(t)\right]. \tag{10}$$

We have found that calorimetric spectra C_v'' reported above closely resemble structural relaxation spectra χ'' based on the self-intermediate scattering function (see Appendix C), supporting that these are generic relaxation spectra. We present our further results based on χ'' which can be obtained more efficiently computationally. Figure 4(a) shows χ'' for conditions similar to those in Fig. 1(a). We observe α and β peaks similar to those from C_v''. As before, we extract both τ_β and τ_α

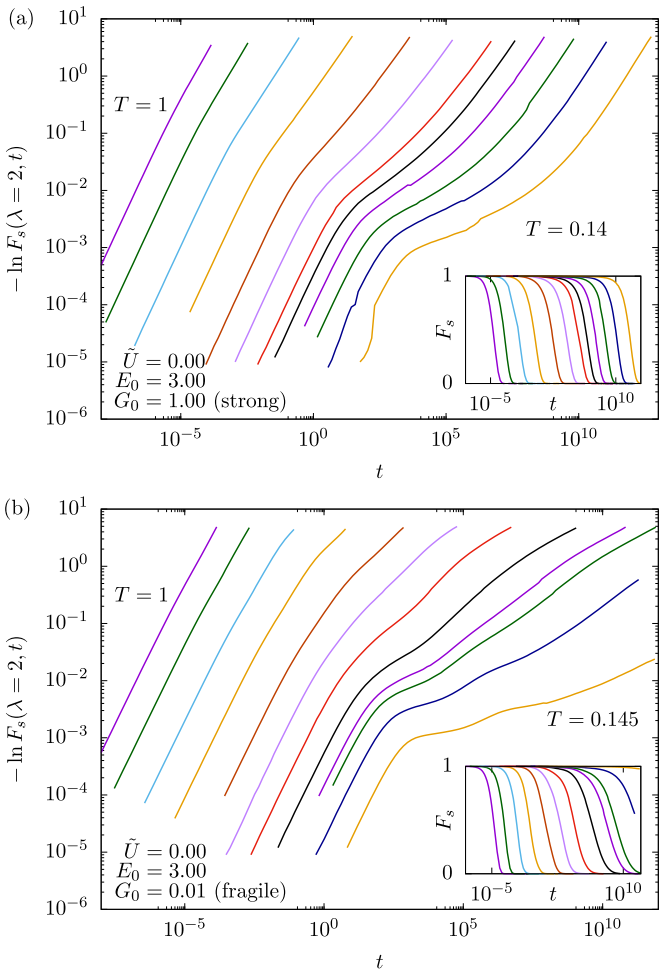

FIG. 3. Plots of $-\ln F_s$ against time t in log-log scale at $\tilde{U} = 0$ and $E_0 = 3$ for moderately strong glass at $G_0 = 1$ and $T = 1, 0.6, 0.4, 0.3, 0.24, 0.21, 0.19, 0.18, 0.17,\quad 0.16, 0.15, 0.14$ from left to right (a) and fragile glass at $G_0 = 0.01$ and $T = 1, 0.6, 0.4, 0.3, 0.24, 0.21, 0.19, 0.175, 0.1667, 0.1626, 0.155, 0.145$ from left to right (b). A T-dependent ϕ_v is adopted. Insets: F_s against time t.

from the spectral peaks. Results are shown in the Arrhenius plot in Fig. 5(a), which qualitatively resemble those of, e.g., $Pd_{40}Ni_{10}Cu_{30}P_{20}$ [54].

Moderately strong glasses have been modeled so far as we have adopted $G_0 = 1$ in Eq. (1). Fragile glass is now considered by taking $G_0 = 0.01$ [35]. Figures 4(b) and 5(b) show χ'' and the relaxation times, respectively, for the same T-dependent void density as in Fig. 4(a). We again observe similar α and β peaks and an Arrhenius plot qualitatively similar to that of, e.g., Toluene [55]. Again, the β peaks can be described on the high-frequency side by the TLS prediction $\chi_{\rm TLS}''$ which equals $C_{\rm TLS}''$ (see Appendix C 1).

D. β_s relaxation rate

Surprisingly, an additional slow β peak, denoted here as β_s, emerges in Fig. 4(b) for $G_0 = 0.01$ at low T in-between the α and the β peaks. It resembles that in some metallic glasses [56], which are typically moderately fragile to

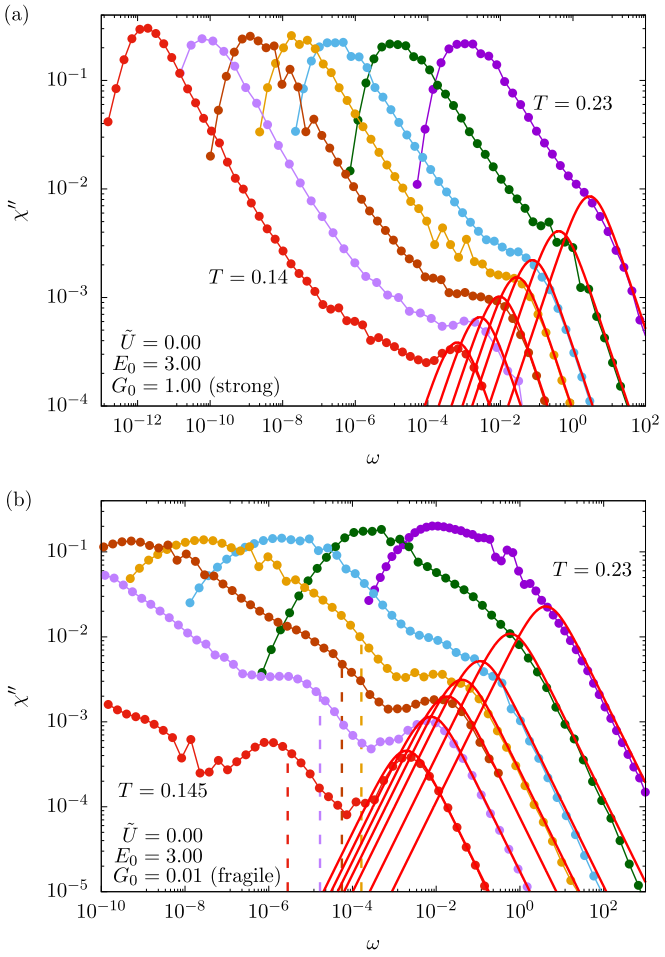

FIG. 4. Structural relaxation spectroscopy at $T = 0.14, 0.15, 0.16, 0.17, 0.18, 0.2, 0.23$ for moderately strong glass with $G_0 = 1$ (a) and $T = 0.145, 0.155, 0.1626, 0.17, 0.18, 0.2, 0.23$ for $G_0 = 0.01$ (b) with a T-dependent void density ϕ_v, $E_0 = 3$, and $\tilde{U} = 0$. We observe α and β peaks in (a) and (b), and β_s peaks in (b). (a), (b) Analytic prediction $\chi''_{\rm TLS}$ (red lines) shows agreement with χ'' at high ω. Dashed vertical lines in (b) show analytic prediction of β_s peak positions.

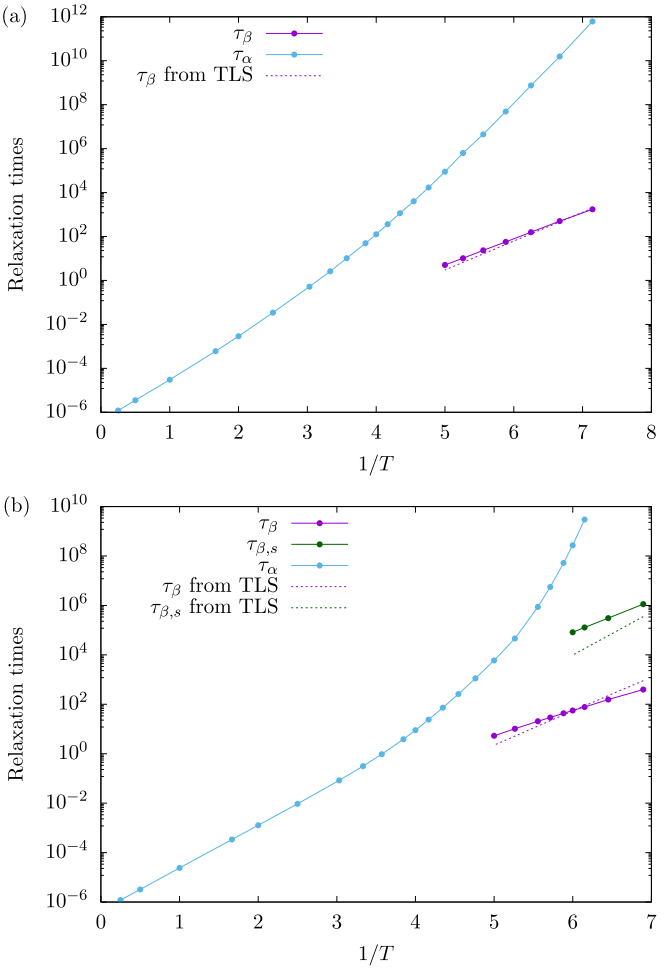

FIG. 5. Arrhenius plots of τ_α and τ_β for moderately strong glass (a) and of τ_α, τ_β, and $\tau_{\beta,s}$ for fragile glass (b) based on peak positions from Figs. 4(a) and 4(b) respectively. The dashed lines show TLS predictions to τ_β and $\tau_{\beta,s}$.

fragile. We denote the relaxation time by $\tau_{\beta,s}$. To understand the relaxation microscopically, Fig. 6 shows the displacement profiles at time $t = 0.4\tau_{\beta,s}$, $\tau_{\beta,s}$, and $1.7\tau_{\beta,s}$ from a simulation at $T = 0.145$, $G_0 = 0.01$, and $E_0 = 3$. They reveal that a significant number of voids have already hopped more than once. This displaces multiple particles, during the period of order $\tau_{\beta,s}$ which is much longer than τ_β. Note that the bimodal distribution in Eq. (1) implies that under conditions of low T and small G_0, the realized pair interactions assume one of two characteristic energy values: a high energy of 0.5 or a low energy of about $k_BT - 0.5$. A β_s relaxation event mainly corresponds to a double hop of a void with the same number of high-energy interactions in the initial and final states (denotes as states 1 and 3) but one extra high-energy interaction in the intermediate barrier state (denotes as state 2). The associated energy change ΔE_{12} or ΔE_{32} when transiting from state 1 or 3 to state 2 follows:

$$\Delta E_{12} \simeq \Delta E_{32} \simeq 1 - k_BT. \tag{11}$$

At state 2, the system quickly deactivates back to state 1 or 3 with nearly equal chances. States 1 and 3 thus form effectively a TLS, which is approximately symmetric. The effective transition rates w_{13} and w_{31} between the two TLS states in either direction follows:

$$w_{13} \simeq w_{31} \simeq w_l(\Delta E_{12})/2, \tag{12}$$

where the factor $\frac{1}{2}$ accounts for the probability that the hop is not reversed after reaching the barrier state. The relaxation rate of such a TLS, which we identify with the β_s peak frequency $\omega_{\beta,s}$, is simply $w_{13} + w_{31}$. Using Eq. (12), we get

$$\omega_{\beta,s} \simeq w_l(\Delta E_{12}) \tag{13}$$

with ΔE_{12} already given in Eq. (11). The rates thus calculated at various T by applying Eq. (2), with no adjustable parameter, are indicated in Fig. 4(b). The results show reasonable agreements with simulations, with the theoretical β_s peak frequency only slightly overestimated. We believe that other contributions such as four-level systems with two barrier states of similar energies slightly slow down the average β_s relaxation rate and shift the β_s peaks towards lower frequencies. Calculated values of relaxation time $\tau_{\beta,s} = 1/\omega_{\beta,s}$ are

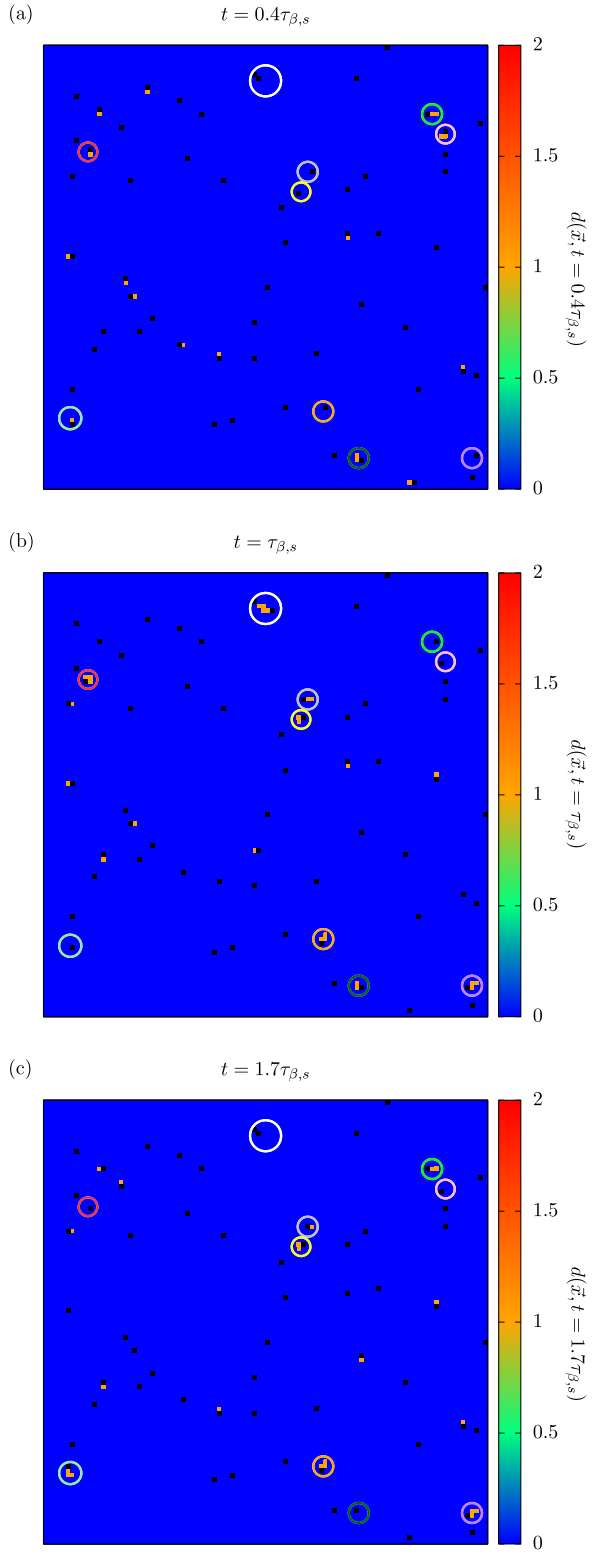

FIG. 6. Spatial displacement profiles $d(\vec{x}, t)$ of particle displacements over time durations $t = 0.4\tau_{\beta,s}$ (a), $\tau_{\beta,s}$ (b), and $1.7\tau_{\beta,s}$ (c) for $G_0 = 0.01$, $\tilde{U} = 0$, $E_0 = 3$ at $T = 0.145$ under the same conditions as in Fig. 4(b). Stationary particles shaded in blue and black squares show the final positions of the voids. Colored circles highlight different locations where each few-level system evolves over time. Up to $t = 1.7\tau_{\beta,s}$, voids involved in the few-level systems are localized and they do not escape further.

also shown in Fig. 5(b) and show reasonable agreements with simulation results. Other fragile glasses, like polymer glasses, may not show a β_s peak. We expect that introducing fluctuations by broadening the δ component in $g(V)$ in Eq. (1) or by increasing $\tilde{U}$ in Eq. (5) can broaden and hence diminish the β_s peak. Note that an observable β_s peak as explained above requires a sharp distribution of the TLS transition barriers as given in Eq. (11). In contrast, it is easy to see that such a feature does not hold for the case of $G_0 \simeq 1$. Consequently, β_s peak is absent in our strong glass results.

III. DISCUSSIONS

The DPLM adopts void-induced particle hops as the only elementary dynamics. It is remarkable that several major spectral features of glass are reproduced. We have explained above that α and β relaxations correspond to single hops of particles and voids, respectively. Such single-hop analogs directly a microstring motion in which a very small number of particles hop simultaneously [28]. The continual diffusion of voids in the DPLM results at long incoherent strings, similar to those in molecular systems [28,29]. Note that the hop of a particle initially far away from a void can take a much longer time than that of a void. This is because the former in general involves two steps: the diffusion of a void to neighbor the particle and then the hop of the particle into the void. Denoting the typical time of this diffusion by τ_{diff}, we have $\tau_\alpha = \tau_{\text{diff}} + \tau_\beta$. As the diffusion in general consists of numerous hops of the void, i.e., numerous β relaxations, $\tau_\alpha \simeq \tau_{\text{diff}} \gg \tau_\beta$. Our results therefore suggest that particle hops in the form of stringlike motions are both α [19,20] and β relaxations [21] as proposed earlier [22], but the whole α process also involves void diffusion. Therefore, β relaxation acts as the precursor and mediator of α relaxation [4,57].

Experiments on glass in general show that the β peak height $C_v''(\omega_\beta)$ is much lower than the height $C_v''(\omega_\alpha)$ of the α peak, with a ratio $C_v''(\omega_\beta)/C_v''(\omega_\alpha)$ often ranges from 0.001 to almost 0.01 across different temperatures for polymers and metallic glasses [4,40]. From Eq. (7) and noting $C_v''(\omega_\alpha) \simeq 1$, we get $C_v''(\omega_\beta)/C_v''(\omega_\alpha) \simeq \phi_v z$. This ratio implies a typical void density $\phi_v \simeq 10^{-4}$ to 0.001 at temperatures with observable β peaks for a coordinate number $z \simeq 10$ in 3D. However, our model cannot at present explain a larger ratio of, e.g., $\sim$1 [4]. and other non-JG mechanisms such as γ realxation [58] and other relaxation of molecular internal degrees of freedom may need to be considered.

Our lattice model approach provides a unified picture not only for α and β relaxations and excess wing but also for a diverse range of glassy phenomena already reproduced in previous DPLM simulations [23,31–39] as the model applied here closely follows definitions used previously. Early lattice model studies focus mainly on explaining the kinetic arrest [59], while a lattice glass model based on particle swap dynamics has very recently reproduced glassy spectra with α and secondary peaks [60]. It will be interesting to test if these models can also reproduce many other glassy phenomena so that consistency among explanations of various features can be scrutinized. In general, lattice models enjoy superior computational efficiency and are highly tractable analytically [59]. In contrast, the best MD spectroscopic simulations can

access the α and β peaks only at different temperatures [21,50].

In Fig. 1, we show the diversity of β peak geometries or excess wings caused by different distributions in the energy barrier offset U_k defined in Eq. (5). The barrier fluctuations may be due to the presence of multiple chemical species or geometrical frustrations in the packing of complex molecules. This agrees with the suggestion that the nature of excess wing is another realization of β relaxation [9,12].

While this study focuses on the DPLM in 2D, our prior work in 3D has characterized key glassy dynamics including particle mean-squared displacement (MSD), diffusion coefficient and its power law relation with the void density, fragility, and self-intermediate scattering function (SISF) [61]. All results show no qualitative difference when compared with their 2D counterparts [23,35]. Given that our dynamical spectroscopy is derived from the SISF, a quantity shown to behave similarly in both dimensions, we anticipate that the qualitative features of the 3D spectroscopy would align with the 2D results reported here.

The DPLM exhibits positional order. Although the model does not account for geometrical frustrations, the underlying physics of frustration is encoded in an energy disorder induced by the random pair interactions. This is supported by a wide range of reported glassy dynamics exhibited by the DPLM [23,31–39], as well as by a recent molecular dynamics simulation study on a glassy crystal, a system possessing positional order but energy disorder which can successfully reproduce glassy dynamics [62].

The DPLM adopts void-induced particle motions, which are closely related to classical ideas of Glarum [63] and Spaepen [64]. Nevertheless, due to the random pair interactions V_{kl} fixed for each atomic pair during a whole simulation, voids in the DPLM diffuse in a nontrivial potential energy landscape, whereas free-volume defects in [63,64] are assumed to follow free diffusion. As a consequence of the nontrivial potential energy landscape, the dynamics in DPLM exhibits emergent facilitation [23] more akin to the Fredrickson-Anderson spin-facilitation model [65–67].

To conclude, we apply calorimetric and structural relaxation spectroscopy to the DPLM to study α relaxation, β relaxation, excess wing, and β_s relaxation, all intuitively understandable based on void-induced particle motions. By increasing the width of particle hopping barrier distribution, β peaks become broadened and eventually become the excess wings. Both α and β relaxations are due to particle hopping motions while the former process also includes the arrival of voids. The temperature dependence of the spectra and, in particular, the relaxation times for both moderately strong and fragile glasses resemble those from experiments.

ACKNOWLEDGMENTS

We thank the support of National Natural Science Foundation of China (Grants No. 12174079 and No. 12404229), Guangdong Basic and Applied Basic Research Foundation (Grant No. 2024A1515011775), and Shenzhen Start-Up Research Funds (Grant No. BL20230925).

DATA AVAILABILITY

The data that support the findings of this article are openly available in [68], embargo periods may apply.

APPENDIX A: ENERGY RELAXATION

The time evolution of the energy relaxation function ϕ_e is given in the inset of Fig. 7 plots. To see its decay more clearly, Fig. 7 shows $-\ln\phi_e$ (solid lines), where a two-step relaxation is well captured.

The second step of the two-step decay of ϕ_e corresponds to αrelaxation and obeys the Kolhrauch-Williams-Watts (KWW) function, i.e., $\phi_e \sim \exp[-(t/\tau_\alpha)^\beta]$. We extract the stretching exponent β as the slope of the tangent of $\ln(-\ln\phi_e)$ against t at $t = \tau_\alpha$, i.e., when $-\ln\phi_e = 1$. The tangents at different T are plotted as dashed lines in Fig. 7, with the values of β also shown. We observe that $\beta \simeq 0.6$ in general and this value is close to 0.5 found in MD simulations [44].

APPENDIX B: VALIDITY OF LINEAR RESPONSE

To support that our reported results lie within the linear regime, we now report additional simulation results with larger temperature perturbations $\delta_T = 10\%$ and 20% at $T = 0.25$ and $G_0 = 1$ and compare them with the original $\delta_T = 6\%$ case. We compute both the calorimetric loss C_v'' and the normalized energy deviation $[e(t) - e_f]/(T_i - T_f)$, where $T_i = T(1 + \delta_T/2)$ and $T_f = (1 - \delta_T/2)$. As shown in Fig. 8, the C_v'' curves for different δ_T nearly collapse, with only a minor deviation for $\delta_T = 20\%$ at the α peak. A similar trend is also observed for the normalized energy deviation reported in the inset of Fig. 8. These results indicate that $\delta_T = 6\%$ and 10% correspond to a linear perturbation regime, whereas simulations with $\delta_T = 20\%$ exhibit discernible nonlinear effects in the α relaxation dynamics with a more stretched relaxation profile. We expect similar conclusions to hold also for other parameter regimes studied in this work.

APPENDIX C: TWO-LEVEL-SYSTEM APPROXIMATION FOR β AND β_s PEAKS

1. β peak in calorimetric relaxation spectrum

At low T, only a small number of particle hopping pathways are energetically favorable [69,70]. For a small void density ϕ_v, most voids may be considered as isolated. We thus assume in this section that only particles neighboring the voids at time $t = 0$ can hop and these hops correspond to short-lived excitations so that they are reversed momentarily. The DPLM then reduces to a set of noninteracting isolated two-level systems (TLSs) at low T and its relaxation spectrum can approximate the β relaxation peak.

Consider particle l neighboring a void at time $t = 0$ in an equilibrium system. At $t > 0$, the particle can either reside at the original position or can hop into the void, forming a TLS. Let E_1 (E_2) be the energy of the TLS when the particle is at the original (hopped) position, with an energy difference $\Delta E = E_1 - E_2$. Denote the probability for the particle to be found at the original position by $p_l(t)$ following $p_l(0) = 1$. The probability to be at the hopped position is then $1 - p_l(t)$.

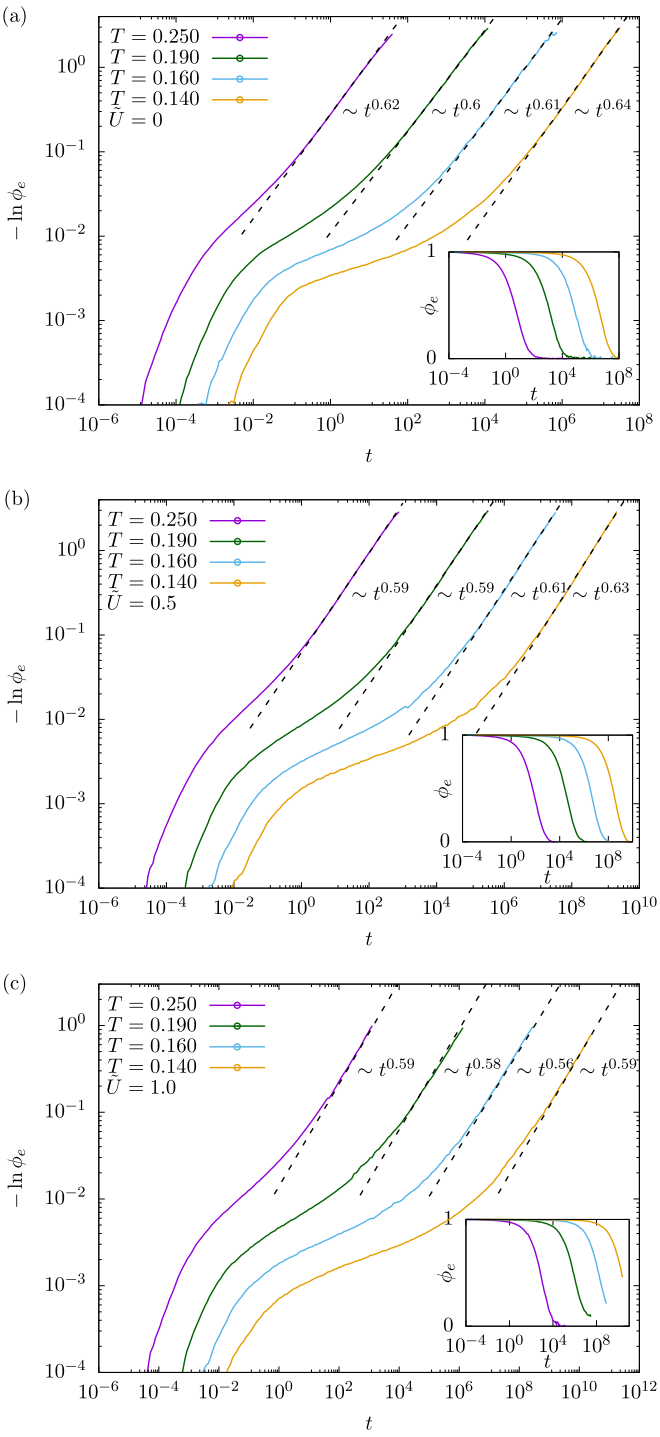

FIG. 7. Plots of $-\ln \phi_e$ versus time t for barrier fluctuation $\tilde{U} = 0$ (a), $\tilde{U} = 0.5$ (b), and $\tilde{U} = 1$ (c) at temperature $T = 0.25, 0.19, 0.16, 0.14$ from left to right for moderately strong glass at $G_0 = 1$ and $E_0 = 1.5$. Insets: ϕ_e against t.

Therefore, $p_l(t)$ follows the rate equation

$$\partial_t p_l(t) = -\mathrm{w}_l(\Delta E) p_l(t) + \mathrm{w}_l(-\Delta E)[1 - p_l(t)], \quad \text{(C1)}$$

where $\mathrm{w}_l(\Delta E)$ is the particle hopping rate given by Eq. (2) and $\mathrm{w}_l(-\Delta E)$ is the backward hopping rate. Solution of

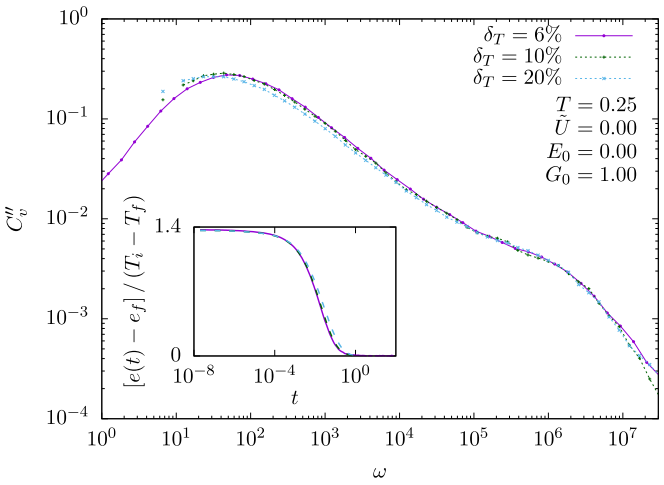

FIG. 8. Calorimetric loss C_v'' at $T = 0.25$, $\tilde{U} = 0$, $E_0 = 0$, and $G_0 = 1$ at different $\delta_T = 6\%$, 10%, and 20%. Inset: $[e(t) - e_f]/(T_i - T_f)$ at different δ_T.

Eq. (C1) is simply given by

$$p_l(t) = p_l(\infty) + [1 - p_l(\infty)] e^{-R_l(\Delta E)t}, \quad \text{(C2)}$$

where $R_l = \mathrm{w}_l(\Delta E) + \mathrm{w}_l(-\Delta E)$ is the relaxation rate of the TLS. In addition, $p_l(\infty)$ is the steady state probability for the particle to be at the original position and we get

$$p_l(\infty) = \frac{\mathrm{w}_l(-\Delta E)}{R_l(\Delta E)}. \quad \text{(C3)}$$

The expected value of the TLS energy at time t is given by

$$E_l(t, \Delta E) = E_1 p_l(t) + E_2[1 - p_l(t)]. \quad \text{(C4)}$$

In our system with L^2 lattice sites and a void density ϕ_v, the total number of particles is $N = (1 - \phi_v)L^2$ and the number of TLS equals $\phi_v z L^2$, where $z = 4$ is the lattice coordination number. We define the energy relaxation function for all particles as

$$\phi_e(t) = \left[1 - \frac{\phi_v z}{(1 - \phi_v)}\right] + \frac{\phi_v z}{(1 - \phi_v)} \left\langle \frac{E_l(t, \Delta E) - E_2}{\Delta E} \right\rangle, \quad \text{(C5)}$$

where the average is taken over all TLS. Here, $\phi_v z/(1 - \phi_v)$ equals the ratio between the number of TLS and the number of particles in the system. This results from averaging over all particles in arriving at Eq. (C5), including those not participating in any TLS. These nonparticipating particles have no contribution to relaxation under the current approximations and are accounted for by the first term in Eq. (C5). Using Eqs. (C4) and (C5), the time derivative of ϕ_e can be calculated and simplified to

$$\dot{\phi}_e(t) = \frac{\phi_v z}{(1 - \phi_v)} \langle \dot{p}_l(t) \rangle. \quad \text{(C6)}$$

By applying Eqs. (4), (C2), and (C6) we get

$$C''_{\mathrm{TLS}}(\omega) = \frac{\phi_v z}{(1 - \phi_v)} \left\langle \frac{\mathrm{w}_l(\Delta E)\omega}{\omega^2 + R_l{}^2(\Delta E)} \right\rangle, \quad \text{(C7)}$$

which is Eq. (7) used in the main text. After formally performing the averaging, we arrive at our final expression for

the numerical evaluation of $C''_{\rm TLS}(\omega)$:

$$C''_{\rm TLS}(\omega) = \frac{\phi_v z}{(1-\phi_v)} \int_{-\infty}^{\infty} d(\Delta E) P(\Delta E) \int_0^{\infty} dU_l f(U_l) \times \frac{\mathrm{w}_l(\Delta E)\omega}{\omega^2 + {R_l}^2(\Delta E)}. \tag{C8}$$

Here, $f(U_l)$ is the probability distribution of the hopping energy barrier offset U_l given by Eq. (5). The probability distribution $P(\Delta E)$ of the energy change ΔE is calculated by numerically taking the convolution over the probability distributions of six interactions, including three newly formed interactions following the *a priori* distributions $g(V)$ and three existing ones following the *a posteriori* distributions $p_{eq}(V, T_i) \sim \exp(-V/k_B T_i) g(V)$ [69], where $k_B = 1$ is the Boltzmann constant.

2. β peak in structural relaxation spectrum

In a TLS, a particle l is either at the origin position with a displacement $\vec{u}_l = \vec{0}$ or it has hopped into the void position with a displacement $\vec{u}_l = \vec{a}$, so that $\vec{a}$ is the relative position between the neighboring sites constituting the TLS. The particle displacement distribution is hence

$$\mathcal{P}(\vec{u}_l, \vec{a}, t, \Delta E) = p_l(t)\delta_{\vec{u}_l,\vec{0}} + [1 - p_l(t)]\delta_{\vec{u}_l,\vec{a}}, \tag{C9}$$

where $p_l(t, \Delta E)$ is given by Eq. (C2) and δ denotes the Kronecker delta. For a wave vector $\vec{k}$,

$$\langle e^{i\vec{k}\cdot\vec{u}_l}\rangle_{\vec{u}_l} = p_l(t) + [1 - p_l(t)]e^{i\vec{k}\cdot\vec{a}}, \tag{C10}$$

where we have only averaged over $\vec{u}_l = 0$ or $\vec{a}$. Taking $\vec{k} = k\hat{i}$ where $\hat{i}$ is a unit lattice vector and averaging over all four possible directions of $\vec{a}$, we get

$$\langle e^{i\vec{k}\cdot\vec{u}_l}\rangle_{\vec{u}_l,\vec{a}} = p_l(t) + [1 - p_l(t)]\left(\tfrac{1}{2}\cos ka + \tfrac{1}{2}\right). \tag{C11}$$

It further reduces to $\langle e^{i\vec{k}\cdot\vec{u}_l}\rangle_{\vec{u}_l,\vec{a}} = p_l(t)$ after substituting $k = 2\pi/\lambda$, $\lambda = 2a$, and $a = 1$. Formally averaging over possible values of ΔE and U_l, our result is finally averaged over all TLSs and we get $\langle e^{i\vec{k}\cdot\vec{u}_l}\rangle = \langle p_l(t)\rangle$. Converting the above average over TLSs to one over particles and taking a time derivative on the result, Eq. (8) becomes

$$\dot{F}_s(t) = \frac{\phi_v z}{(1-\phi_v)} \langle \dot{p}_l(t)\rangle, \tag{C12}$$

which is directly analogous to Eq. (C6). Finally, using Eqs. (10), (C2), and (C12) and comparing the result with Eq. (7), the structural relaxation spectrum $\chi''_{\rm TLS}$ under the TLS approximation follows

$$\chi''_{\rm TLS} = C''_{\rm TLS} \tag{C13}$$

as reported in the main text.

3. The most probable hopping rate of successful hops of voids

We will now relate the β relaxation rate ω_β with the void hopping rate by showing that

$$\omega_\beta \simeq \hat{\mathrm{w}}, \tag{C14}$$

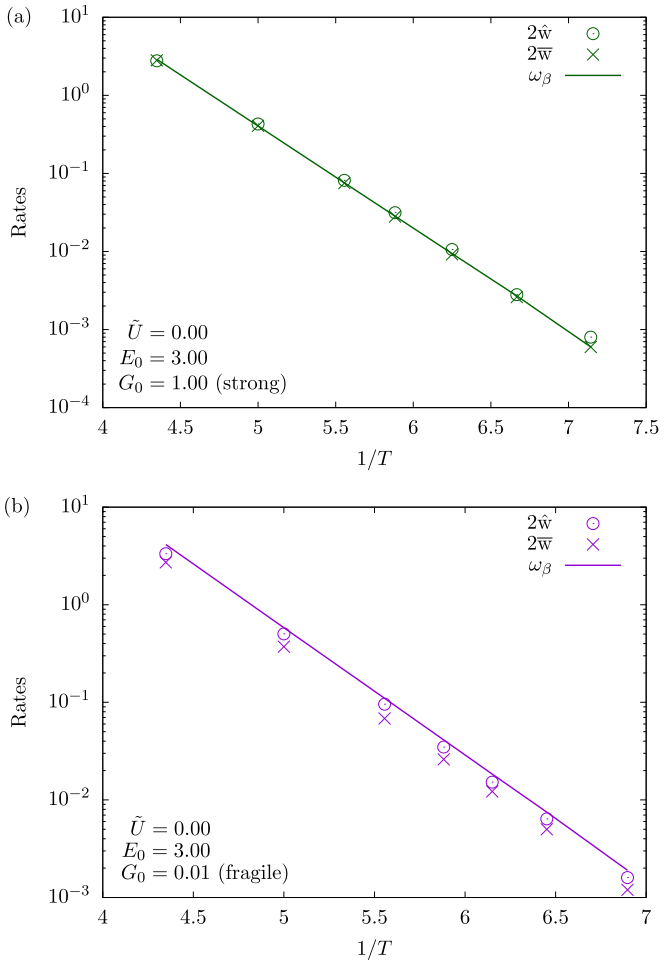

FIG. 9. Arrhenius plot of $2\hat{\mathrm{w}}$, $2\overline{\mathrm{w}}$ and ω_β for $G_0 = 1$ (a) and $G_0 = 0.01$ (b), respectively. Values of ω_β are from maximizing Eq. (C8).

where $\hat{\mathrm{w}}$ denotes the most probable hopping rate of the successful hops of voids. We emphasize that $\hat{\mathrm{w}}$ concerns successful hops and can be obtained by, for example, examining hops of voids which have occurred during a period of simulation. This is distinct from considering all possible hops of voids, many of which can be energetically unfavorable and contribute little to the statistics.

The analysis applies for both $C''_{\rm TLS}(\omega)$ and $\chi''_{\rm TLS}(\omega)$. For simplicity, our discussion focuses only on the former. We rewrite Eq. (C8) as

$$C''_{\rm TLS}(\omega) = \frac{\phi_v z}{(1-\phi_v)} \int_{-\infty}^{\infty} d(\Delta E) P(\Delta E) \int_0^{\infty} dU_l f(U_l) \times \frac{\mathrm{w}_l(\Delta E)}{2R_l(\Delta E)} g(\omega), \tag{C15}$$

where

$$g(\omega) = \frac{2R_l(\Delta E)\omega}{\omega^2 + {R_l}^2(\Delta E)}. \tag{C16}$$

Here, the function $g(\omega)$ has a single peak of value 1 located at $\omega = R_l(\Delta E)$. Assuming that narrowing down the peak width of $g(\omega)$ may not shift the β peak position ω_β significantly, we take the rough approximation that $g(\omega) \propto \delta[\omega - R_l(\Delta E)]$, where $\delta(\cdot)$ denotes the Dirac delta function. We also neglect

the dependence of $R_l(\Delta E)$ on ΔE and U_l, which is much weaker compared with that of $\mathrm{w}_l(\Delta E)$. We get

$$C''_{\mathrm{TLS}}(\omega) \propto \int_{-\infty}^{\infty} d(\Delta E) P(\Delta E) \int_0^{\infty} dU_l f(U_l) \times \mathrm{w}_l(\Delta E)\delta[\omega - R_l(\Delta E)]. \quad \text{(C17)}$$

Noting that the integrand is dominated by small ΔE satisfying $\|\Delta E\| \lesssim k_B T$, we have $\mathrm{w}_l(\Delta E) \simeq \mathrm{w}_l(-\Delta E)$ so that $R_l(\Delta E) \simeq 2\mathrm{w}_l(\Delta E)$. Therefore, we get

$$C''_{\mathrm{TLS}}(\omega) \propto \int_{-\infty}^{\infty} d(\Delta E) P(\Delta E) \int_0^{\infty} dU_l f(U_l) \times \mathrm{w}_l(\Delta E)\delta[\omega - 2\mathrm{w}_l(\Delta E)]. \quad \text{(C18)}$$

On the other hand, the probability distribution $\Psi(\mathrm{w})$ of the hopping rate w of successful hopping events of voids, i.e., of particles hopping into neighboring voids, is given by

$$\Psi(\mathrm{w}) = \frac{1}{\mathcal{N}_{\mathrm{w}}} \int_{-\infty}^{\infty} d(\Delta E) P(\Delta E) \int_0^{\infty} dU_l f(U_l) \times \mathrm{w}_l(\Delta E)\, \delta[\mathrm{w} - \mathrm{w}_l(\Delta E)], \quad \text{(C19)}$$

where $\mathcal{N}_{\mathrm{w}}$ is a normalization constant. A factor $\mathrm{w}_l(\Delta E)$ in the integrand accounts for the relative probability that a possible hop occurs successfully. Comparing Eqs. (C18) and (C19), we find

$$C''_{\mathrm{TLS}}(2\mathrm{w}) \propto \Psi(\mathrm{w}). \quad \text{(C20)}$$

Hence, the peak position ω_β of $C''_{\mathrm{TLS}}(\omega)$ follows:

$$\omega_\beta \simeq 2\hat{\mathrm{w}}, \quad \text{(C21)}$$

where $\hat{\mathrm{w}}$ maximizes $\Psi(\mathrm{w})$ and is thus the most probable hopping rate of successful hops of voids in the system. Equation (C21) can be simplified to Eq. (C14), as the factor 2 is in most cases negligible. In addition, $\hat{\mathrm{w}}$ can further be approximated by the average hopping rate $\bar{\mathrm{w}}$ of successful hops of voids, i.e., $\hat{\mathrm{w}} \simeq \bar{\mathrm{w}}$. Equation (C21) then implies

$$\omega_\beta \simeq 2\bar{\mathrm{w}}. \quad \text{(C22)}$$

To verify that Eqs. (C21) and (C22) are consistent with ω_β from the more accurate expression of $C''_{\mathrm{TLS}}(\omega)$ in Eq. (C8), we have performed DPLM simulations in which we record the hopping rate w of each successful hop of a particle into a void. Its probability distribution $\Psi(\mathrm{w})$ is measured. The most probable value $\hat{\mathrm{w}}$ and the average $\bar{\mathrm{w}}$ are computed. Figure 9 compares ω_β with $\hat{\mathrm{w}}$ and $\overline{w}$ for both fragile ($G_0 = 0.01$) and strong ($G_0 = 1$) cases, verifying Eqs. (C21) and (C22) and justifying the δ-function approximation we have taken on $g(\omega)$.

[1] D. Chandler and J. P. Garrahan, Dynamics on the way to forming glass: Bubbles in space-time, Annu. Rev. Phys. Chem. **61**, 191 (2010).

[2] G. Biroli and J. P. Garrahan, Perspective: The glass transition, J. Chem. Phys. **138**, 12A301 (2013).

[3] F. Arceri, F. P. Landes, L. Berthier, and G. Biroli, Glasses and aging, a statistical mechanics perspective on, in *Statistical and Nonlinear Physics* (Springer, Berlin, 2022), p. 229.

[4] K. Ngai, *Relaxation and Diffusion in Complex Systems*, Partially Ordered Systems (Springer, Berlin, 2011).

[5] W. H. Wang, Dynamic relaxations and relaxation-property relationships in metallic glasses, Prog. Mater. Sci. **106**, 100561 (2019).

[6] A. Zaccone, *Theory of Disordered Solids: From Atomistic Dynamics to Mechanical, Vibrational, and Thermal Properties*, Lecture Notes in Physics, Vol. 1015 (Springer, Cham, 2023).

[7] H. E. Taylor, The dielectric relaxation spectrum of glass, Trans. Faraday Soc. **52**, 873 (1956).

[8] G. P. Johari and M. Goldstein, Viscous liquids and the glass transition. II. Secondary relaxations in glasses of rigid molecules, J. Chem. Phys. **53**, 2372 (1970).

[9] H. B. Yu, W. H. Wang, H. Y. Bai, and K. Samwer, The β-relaxation in metallic glasses, Natl. Sci. Rev. **1**, 429 (2014).

[10] S. Hensel-Bielówka, M. Paluch, and K. L. Ngai, Emergence of the genuine Johari–Goldstein secondary relaxation in m-fluoroaniline after suppression of hydrogen-bond-induced clusters by elevating temperature and pressure, J. Chem. Phys. **123**, 014502 (2005).

[11] Y. Gao, Z. Chen, W. Tu, X. Li, Y. Tian, R. Liu, and L.-M. Wang, Anomaly in dielectric relaxation dispersion of glass-forming alkoxy alcohols, J. Chem. Phys. **142**, 214505 (2015).

[12] U. Schneider, R. Brand, P. Lunkenheimer, and A. Loidl, Excess wing in the dielectric loss of glass formers: A Johari-Goldstein β relaxation? Phys. Rev. Lett. **84**, 5560 (2000).

[13] J. P. Gabriel, P. Zourchang, F. Pabst, A. Helbling, P. Weigl, T. Böhmer, and T. Blochowicz, Intermolecular cross-correlations in the dielectric response of glycerol, Phys. Chem. Chem. Phys. **22**, 11644 (2020).

[14] J. Qiao, J.-M. Pelletier, and R. Casalini, Relaxation of bulk metallic glasses studied by mechanical spectroscopy, J. Phys. Chem. B **117**, 13658 (2013).

[15] H. B. Yu, K. Samwer, W. H. Wang, and H. Y. Bai, Chemical influence on β-relaxations and the formation of molecule-like metallic glasses, Nat. Commun. **4**, 2204 (2013).

[16] C. Scalliet, B. Guiselin, and L. Berthier, Thirty milliseconds in the life of a supercooled liquid, Phys. Rev. X **12**, 041028 (2022).

[17] M. R. Hasyim and K. K. Mandadapu, Emergent facilitation and glassy dynamics in supercooled liquids, Proc. Natl. Acad. Sci. USA **121**, e2322592121 (2024).

[18] L. Costigliola, T. Hecksher, and J. C. Dyre, Glass-forming liquids need facilitation, Proc. Natl. Acad. Sci. USA **121**, e2408798121 (2024).

[19] C. Donati, J. F. Douglas, W. Kob, S. J. Plimpton, P. H. Poole, and S. C. Glotzer, Stringlike cooperative motion in a supercooled liquid, Phys. Rev. Lett. **80**, 2338 (1998).

[20] A. S. Keys, L. O. Hedges, J. P. Garrahan, S. C. Glotzer, and D. Chandler, Excitations are localized and relaxation is hierarchical in glass-forming liquids, Phys. Rev. X **1**, 021013 (2011).

[21] H.-B. Yu, R. Richert, and K. Samwer, Structural rearrangements governing Johari-Goldstein relaxations in metallic glasses, Sci. Adv. **3**, e1701577 (2017).

[22] C.-H. Lam, Repetition and pair-interaction of string-like hopping motions in glassy polymers, J. Chem. Phys. **146**, 244906 (2017).

[23] L.-H. Zhang and C.-H. Lam, Emergent facilitation behavior in a distinguishable-particle lattice model of glass, Phys. Rev. B **95**, 184202 (2017).

[24] D. Cangialosi, V. M. Boucher, A. Alegria, and J. Colmenero, Free volume holes diffusion to describe physical aging in poly (mehtyl methacrylate)/silica nanocomposites, J. Chem. Phys. **135**, 014901 (2011).

[25] C.-T. Yip, M. Isobe, C.-H. Chan, S. Ren, K.-P. Wong, Q. Huo, C.-S. Lee, Y.-H. Tsang, Y. Han, and C.-H. Lam, Direct evidence of void-induced structural relaxations in colloidal glass formers, Phys. Rev. Lett. **125**, 258001 (2020).

[26] B. Mei, B. Zhuang, Y. Lu, L. An, and Z.-G. Wang, Local-average free volume correlates with dynamics in glass formers, J. Phys. Chem. Lett. **13**, 3957 (2022).

[27] Y.-D. Wang, C. Xiao, A. Kumar, Y.-H. Shi, C.-S. Lee, K.-C. Lam, M.-K. Fung, C.-H. Chan, Y.-H. Tsang, B. Li, C.-H. Lam, and C.-T. Yip, Direct manipulation of diffusion in colloidal glasses via controlled generation of quasi-particle-like defects, Phys. Rev. E **110**, 064603 (2024).

[28] Y. Gebremichael, M. Vogel, and S. C. Glotzer, Particle dynamics and the development of string-like motion in a simulated monoatomic supercooled liquid, J. Chem. Phys. **120**, 4415 (2004).

[29] P. M. Derlet and R. Maaß, Micro-plasticity in a fragile model binary glass, Acta Mater. **209**, 116771 (2021).

[30] P. M. Derlet, H. Bocquet, and R. Maaß, Viscosity and transport in a model fragile metallic glass, Phys. Rev. Mater. **5**, 125601 (2021).

[31] C.-S. Lee, H.-Y. Deng, C.-T. Yip, and C.-H. Lam, Large heat-capacity jump in cooling-heating of fragile glass from kinetic monte carlo simulations based on a two-state picture, Phys. Rev. E **104**, 024131 (2021).

[32] M. Lulli, C.-S. Lee, L.-H. Zhang, H.-Y. Deng, and C.-H. Lam, Kovacs effect in glass with material memory revealed in non-equilibrium particle interactions, J. Stat. Mech. (2021) 093303.

[33] X.-Y. Gao, H.-Y. Deng, C.-S. Lee, J. You, and C.-H. Lam, Emergence of two-level systems in glass formers: A kinetic monte carlo study, Soft Matter **18**, 2211 (2022).

[34] X.-Y. Gao, C.-Y. Ong, C.-S. Lee, C.-T. Yip, H.-Y. Deng, and C.-H. Lam, Kauzmann paradox: A possible crossover due to diminishing local excitations, Phys. Rev. B **107**, 174206 (2023).

[35] C.-S. Lee, M. Lulli, L.-H. Zhang, H.-Y. Deng, and C.-H. Lam, Fragile glasses associated with a dramatic drop of entropy under supercooling, Phys. Rev. Lett. **125**, 265703 (2020).

[36] M. Lulli, C.-S. Lee, H.-Y. Deng, C.-T. Yip, and C.-H. Lam, Spatial heterogeneities in structural temperature cause kovacs' expansion gap paradox in aging of glasses, Phys. Rev. Lett. **124**, 095501 (2020).

[37] G. Gopinath, C.-S. Lee, X.-Y. Gao, X.-D. An, C.-H. Chan, C.-T. Yip, H.-Y. Deng, and C.-H. Lam, Diffusion-coefficient power laws and defect-driven glassy dynamics in swap acceleration, Phys. Rev. Lett. **129**, 168002 (2022).

[38] C.-Y. Ong, C.-S. Lee, X.-Y. Gao, Q. Zhai, Z. Yu, R. Shi, H.-Y. Deng, and C.-H. Lam, Relating fragile-to-strong transition to fragile glass via lattice model simulations, Phys. Rev. E **109**, 054124 (2024).

[39] Q. Zhai, X.-Y. Gao, C.-S. Lee, C.-Y. Ong, K. Yan, H.-Y. Deng, S. Yang, and C.-H. Lam, Surface mobility gradient and emergent facilitation in glassy films, Soft Matter **20**, 4389 (2024).

[40] K. Niss and T. Hecksher, Perspective: Searching for simplicity rather than universality in glass-forming liquids, J. Chem. Phys. **149**, 230901 (2018).

[41] T. V. Tropin, J. W. P. Schmelzer, G. Schulz, and C. Schick, The calorimetric glass transition in a wide range of cooling rates and frequencies, in *The Scaling of Relaxation Processes*, edited by F. Kremer and A. Loidl (Springer, Cham, 2018), p. 307.

[42] Q. Zheng, Y. Zhang, M. Montazerian, O. Gulbiten, J. C. Mauro, E. D. Zanotto, and Y. Yue, Understanding glass through differential scanning calorimetry, Chem. Rev. **119**, 7848 (2019).

[43] A. J. Kovacs, Transition vitreuse dans les polymères amorphes. Etude phénoménologique, in *Fortschritte Der Hochpolymeren-Forschung* (Springer, Berlin, 1964), p. 394.

[44] F. Pabst, J. P. Gabriel, T. Böhmer, P. Weigl, A. Helbling, T. Richter, P. Zourchang, T. Walther, and T. Blochowicz, Generic structural relaxation in supercooled liquids, J. Phys. Chem. Lett. **12**, 3685 (2021).

[45] T. Hecksher, D. H. Torchinsky, C. Klieber, J. A. Johnson, J. C. Dyre, and K. A. Nelson, Toward broadband mechanical spectroscopy, Proc. Natl. Acad. Sci. USA **114**, 8710 (2017).

[46] B. Ruta, Y. Chushkin, G. Monaco, L. Cipelletti, E. Pineda, P. Bruna, V. M. Giordano, and M. Gonzalez-Silveira, Atomic-scale relaxation dynamics and aging in a metallic glass probed by x-ray photon correlation spectroscopy, Phys. Rev. Lett. **109**, 165701 (2012).

[47] Z. Evenson, B. Ruta, S. Hechler, M. Stolpe, E. Pineda, I. Gallino, and R. Busch, X-ray photon correlation spectroscopy reveals intermittent aging dynamics in a metallic glass, Phys. Rev. Lett. **115**, 175701 (2015).

[48] A. Das, P. M. Derlet, C. Liu, E. M. Dufresne, and R. Maaß, Stress breaks universal aging behavior in a metallic glass, Nat. Commun. **10**, 5006 (2019).

[49] M. Goldstein, Viscous liquids and the glass transition: A potential energy barrier picture, J. Chem. Phys. **51**, 3728 (1969).

[50] Y. Sun, S.-X. Peng, Q. Yang, F. Zhang, M.-H. Yang, C.-Z. Wang, K.-M. Ho, and H.-B. Yu, Predicting complex relaxation processes in metallic glass, Phys. Rev. Lett. **123**, 105701 (2019).

[51] T. Damart and D. Rodney, Atomistic study of two-level systems in amorphous silica, Phys. Rev. B **97**, 014201 (2018).

[52] K. Friedrich and S. Andreas, *Broadband Dielectric Spectroscopy* (Springer-Verlag, Berlin Heidelberg, 2003).

[53] K. Vollmayr-Lee, Single particle jumps in a binary lennard-jones system below the glass transition, J. Chem. Phys. **121**, 4781 (2004).

[54] H.-B. Yu, W.-H. Wang, and K. Samwer, The β relaxation in metallic glasses: An overview, Mater. Today **16**, 183 (2013).

[55] A. Kudlik, C. Tschirwitz, T. Blochowicz, S. Benkhof, and E. Rössler, Slow secondary relaxation in simple glass formers, J. Non-Cryst. Solids **235-237**, 406 (1998).

[56] Q. Luo, L. Shao, L. Xue, J. Cui, Q. Yang, J. Wang, H. Ke, B. Shen, and W. Wang, Medium-range imperfect order determining the slow β-relaxation in metallic glasses, Sci. China Mater. **67**, 983 (2024).

[57] J. S. Harmon, M. D. Demetriou, W. L. Johnson, and K. Samwer, Anelastic to plastic transition in metallic glass-forming liquids, Phys. Rev. Lett. **99**, 135502 (2007).

[58] S. Küchemann and R. Maaß, Gamma relaxation in bulk metallic glasses, Scr. Mater. **137**, 5 (2017).

[59] J. P. Garrahan, P. Sollich, and C. Toninelli, Kinetically constrained models, in *Dynamical Heterogeneities in Glasses, Colloids and Granular Media*, edited by L. Berthier, G. Biroli, J.-P. Bouchaud, L. Cipelletti, and W. van Saarloosand (Oxford University Press, Oxford, 2011).

[60] Y. Nishikawa and L. Berthier, Collective relaxation dynamics in a three-dimensional lattice glass model, Phys. Rev. Lett. **132**, 067101 (2024).

[61] B. Li, C.-S. Lee, X.-Y. Gao, H.-Y. Deng, and C.-H. Lam, The distinguishable-particle lattice model of glasses in three dimensions, Soft Matter **20**, 1009 (2024).

[62] L. S. I. Lam, G. Gopinath, Z. Zhao, S. Wang, C.-S. Lee, H.-Y. Deng, F. Wang, Y. Han, C.-T. Yip, and C.-H. Lam, Distinguishable-particle glassy crystal: The simplest molecular model of glass, J. Chem. Phys. **163**, 024505 (2025).

[63] S. H. Glarum, Dielectric relaxation of isoamyl bromide, J. Chem. Phys. **33**, 639 (1960).

[64] F. Spaepen, A microscopic mechanism for steady state inhomogeneous flow in metallic glasses, Acta Metall. **25**, 407 (1977).

[65] G. H. Fredrickson and H. C. Andersen, Kinetic Ising model of the glass transition, Phys. Rev. Lett. **53**, 1244 (1984).

[66] G. H. Fredrickson and H. C. Andersen, Facilitated kinetic Ising models and the glass transition, J. Chem. Phys. **83**, 5822 (1985).

[67] G. H. Fredrickson and S. A. Brawer, Monte Carlo investigation of a kinetic Ising model of the glass transition, J. Chem. Phys. **84**, 3351 (1986).

[68] C.-S. Lee, H. Deng, L. Zhang, C. Xiao, B. Li, C.-T. Yip, and C.-H. Lam, Processed data for the manuscript: A unified picture of structural relaxation, beta relaxation and excess wing in glass formers (2025), https://figshare.com/articles/dataset/Calorimetric_spectrum_processed_data/28931765.

[69] C.-H. Lam, Local random configuration-tree theory for string repetition and facilitated dynamics of glass, J. Stat. Mech. (2018) 023301.

[70] H.-Y. Deng, C.-S. Lee, M. Lulli, L.-H. Zhang, and C.-H. Lam, Configuration-tree theoretical calculation of the mean-squared displacement of particles in glass formers, J. Stat. Mech. (2019) 094014.